Structure-Property Correlation behind the High Mobility of Carbazolocarbazole

*Miriam Más-Montoya,[‡] ‖ Stamatis Georgakopoulos,[‡] José Pedro Cerón-Carrasco,[†] José Pérez,[§] Alberto Tárraga[‡] and David Curiel[‡]**

[‡] Department of Organic Chemistry, Faculty of Chemistry, University of Murcia, Campus of Espinardo, 30100-Murcia, Spain.
[†] Bioinformatics and High Performance Computing Group, Universidad Católica San Antonio de Murcia (UCAM), Avda. Jerónimos, 135, 30107 Guadalupe, Murcia, Spain.
[§] Departamento de Ingeniería Minera, Geológica y Cartográfica, Área de Química Inorgánica, Regional Campus of International Excellence "Campus Mare Nostrum", Universidad Politécnica de Cartagena, 30203 Cartagena, Spain.

KEYWORDS. Carbazolocarbazole, azaphenacene, organic semiconductor, thin film transistor.

ABSTRACT. A comparative study of carbazolocarbazole isomers and their respective *N*-alkyl derivatives confirms the good performance of carbazolo[2,1-*a*]carbazole as hole transporting material in organic field effect transistors. The azaphenacene structure of this molecule forms a dense packing promoted by particularly short longitudinal shifts between molecules establishing face-to-face and edge-to-face interactions. Computational calculations have determined an almost isotropic 2D transport environment within a lamellar structure. This favorable solid state arrangement, in combination with appropriate interfacial layers, has led to a high mobility (1.3 $cm^2V^{-1}s^{-1}$) that validates the aptitude of this molecular material as organic semiconductor.

INTRODUCTION

The area of organic electronics has experienced a remarkable progress in the last few decades motivated by the objective of developing a new generation of optoelectronic devices with technical properties as appealing as flexibility, lightness and reduced manufacturing cost.[1, 2] To a great extent, the design and synthesis of numerous materials have enabled the continuous improvement in the performance of devices such as organic field-effect transistors (OFETs), organic light-emitting devices (OLEDs) or organic solar cells (OSCs), to mention just the more representative ones.[3] Polycyclic aromatic and heteroaromatic systems represent one of the series of molecules that has supplied with some of the best results among the organic semiconductors in terms of charge carrier mobility.[4] In this regard, we focus our attention on the study of fused hexacyclic systems, such as carbabazolocarbazoles, in field-effect transistors. Besides, despite the unquestionable connection between the molecular structure and the charge transport ability of the organic semiconductors, the correlation between the properties at the molecular scale, some of them with a quantum origin,[5] and the material properties at a much larger scale becomes a challenging task, especially when this implies the use of amorphous or polycrystalline thin films.[6] The geometry, atomic composition[7] and functionalization of fused aromatic systems[8] determine their electronic structure and solid state packing.[9] Additionally, some other aspects like the processing protocol[10] and the multilayer architecture of the devices, with special emphasis on the dielectric interface,[11] can affect the morphology of the thin films.[12] Finally, it is the combination of all these features that will determine the charge transport ability of organic semiconductors. Although intense theoretical research is currently being carried out to reinforce the predictability of the charge transport properties from the molecular structure,[13] this approach has to be further developed. Therefore, a meticulous experimental research on the synthetic materials is still required. In the end, the combined studies from the theoretical and experimental side will provide with more data that will permit the development of predicting methods and a better understanding of the structure-property correlation.[4b, 14] In this regard, we want to report the progress of our work in the series of carbazolocarbazoles

whose hexacyclic structure results from the fusion of two carbazole units.[15] Particularly, we have studied in detail the effect of isomerism, as well as *N*-alkylation, on the crystal packing, thin film morphology and charge transport properties of these materials. The impact of isomerism on solid state packing and subsequently on charge mobility has become an interesting aspect to look at as it can be inferred from recent studies.[16] In this regard, our investigation about the synthesis and processing of carbazolocarbazoles has allowed us to optimize materials and devices that have reached hole mobilities as high as 1.3 $cm^2V^{-1}s^{-1}$ in OFETs, which represent the highest mobility reported within the family of pyrrole-based azaphenacenes in thin film transistors.[17] We will focus our attention on the structures of carbazolo[2,1-*a*]carbazole, **1**, carbazolo[4,3-*c*]carbazole, **3** and their corresponding *N*-alkylated derivatives, **2** and **4** (Figure 1). Differently from the family of azaacenes, consisting in the linear attachment of benzene and six-membered azaheterocycles,[18] the integration of a five-membered ring such as pyrrole into the polyheteroaromatic system results in an angular ring fusion typical of isolectronic phenacene or phene structures.[19] In the case of isomers **1** and **3**, they have a close structural relation since both result from the fusion of the central naphthalene through its C1-C2 and C5-C6 bonds with the indole side units. Therefore, both isomers have a centrosymmetric structure but with different angular orientations that exemplify how subtle changes in the molecular structure can have a great impact on the charge transport properties. The dissimilarly oriented indole units would classify them as azaphenacene o azaphene systems. In the case of carbazolo[2,1-*a*]carbazole, it is isoelectronic to fulminene and the more sigmoidal geometry of carbazolo[4,3-*c*]carbazole relates to the isoelectronic dibenzo[*c*,*l*]chrysene.

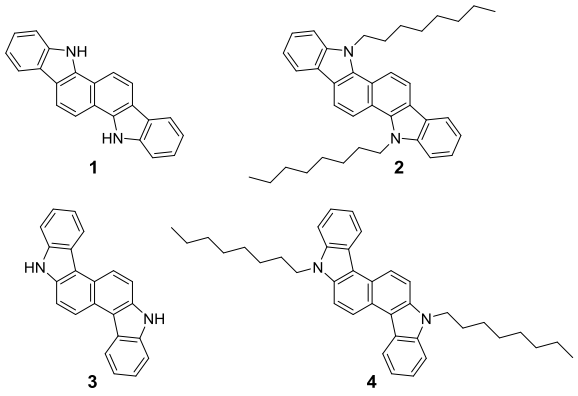

Figure 1. Carbazolo[2,1-*a*]carbazole derivatives, **1** and **2**, and carbazolo[4,3-*c*]carbazole derivatives, **3** and **4**.

EXPERIMENTAL

General. Reagents used as starting materials were purchased from commercial sources and were used without further purification. Solvents were dried following the usual protocols. Unless stated otherwise, all reactions were carried out under nitrogen atmosphere. Carbazolo[2,1-*a*]carbazole, carbazolo[4,3-*c*]carbazole and 1,8-dioctylcarbazolo[4,3-*c*]carbazole were synthesized as reported elsewhere.[15c, 15e] Column chromatography was run with silica gel 60 A CC 70-200 μm as stationary phase using HPLC grade solvents. The final purification of the materials was performed by gradient sublimation under high vacuum conditions (<10^{-6} mbar). Melting points were measured in a Reichert instrument and are not corrected. Unless stated otherwise, all spectra were recorded at room temperature. ^{1}H-NMR and ^{13}C-NMR spectra were recorded on a Bruker AV300 spectrometers having frequencies of 300 MHz for proton nuclei and 75 MHz for carbon nuclei, respectively. Chemical shifts are referred to the residual peak from the deuterated solvent. Mass spectrometry was recorded on HPLC-MS TOF 6220 instrument. Absorption spectra were recorded on a Cary 5000 UV-vis-NIR spectrophotometer. Cyclic voltammetry was recorded utilizing a Bass potenciostate. Platinum working electrode and SCE reference electrode were used for the measurements in solution, whereas boron-doped diamond working electrode and Ag/AgCl reference electrode (using ferrocene as internal standard) were used for the experiments with solid state samples. In both cases platinum wire was used as counter-electrode.

Synthesis of 7,14-dioctylcarbazolo[2,1-*a*]carbazole, 2: Over a solution of carbazolo[2,1-*a*]carbazole (0.4 g, 1.31 mmol) in *N*,*N*-dimethylformamide (30 mL), KOH (0.44 g, 7.8 mmol) and 1-bromooctane (2.52 g, 13.1 mmol) were sequentially added. The reaction mixture was stirred overnight at 60 °C. After cooling to room temperature, the solvent was evaporated under reduced pressure and the crude was precipitated in methanol and thoroughly washed with water. After drying under vacuum, the crude product was purified by column chromatography on silica gel eluting with

dichloromethane:hexane (1:2) and precipitated in methanol to obtain **2** as a white solid (0.48 g, 70%). The isolated solid was further purified by gradient sublimation under high vacuum conditions. M. p.: 125-127 °C. ^{1}H NMR (300 MHz, $CDCl_3$, δ): 8.39 (d, *J* = 8.7 Hz, 2H), 8.31 (d, *J* = 8.8 Hz, 2H), 8.21 (d, *J* = 7.7 Hz, 2H), 7.50-7.61 (m, 4H), 7.32-7.37 (m, 2H), 4.83 (t, *J* = 8.1 Hz, 4H), 2.10 - 2.21 (m, 4H), 1.54 - 1.64 (m, 4H), 1.28 - 1.47 (m, 16H), 0.88 - 0.92 (m, 6H). ^{13}C NMR (75 MHz, $CDCl_3$, ppm, δ): 141.1, 140.0, 136.4, 125.0, 123.1, 121.7, 119.7, 118.8, 118.4, 114.3, 109.4, 46.7, 32.0, 30.3, 29.5, 29.4, 27.3, 22.8, 14.3. HRMS (ESI-TOF) *m/z*: $[M+H]^+$ calcd. for $C_{38}H_{47}N_2$ 531.3734, found 531.3726.

X-ray diffraction and thin film morphology: The single-crystal X-ray data were collected at 100 K with a Bruker D8Quest Kappa Diffractometer using CuKα radiation. The structure was solved using direct methods and refined on F2 by full-matrix least-squares method, using SHELX-2013 software package and expanded using Fourier techniques. All non-hydrogen atoms were refined anisotropically. Hydrogen atoms were found by Fourier difference map and were treated as a riding model except to N1H01 that was refined as free with Dfix.

CCDC numbers for the crystal structures are: **1** (1522122), **2** (1549634), **3** (905793) and **4** (905794).

Thin film X-ray diffraction data were collected on a Bruker D8 Advance instrument in θ-θ mode with CuKα radiation (wavelength 1.54060 Å), 40 kV, 30 mA, and a 1-dimensional detector with a window of 1°. Primary optics consisted of a 2° Soller slit, a 1 mm incidence slit, and an air scatter screen. Secondary optics included a 3 mm antiscatter slit, a Ni filter and a 2.5° Soller slit. Sample was step scanned from 3 to 65° in 2th, with 0.05° stepping intervals, 1 s per step, and a rotation speed of 30 rpm.

AFM measurements were performed on a NT-MDT microscope (NTEGRA PRIMA) in tapping mode and images were analyzed with Gwyddion V2.47.

OFETs fabrication and characterization: P-doped n++ silicon wafers covered with 300 nm thermally grown SiO_2 were cleaned by sequentially immersing in water, acetone and isopropanol in an ultrasonic bath for 20 min. Subsequently, a coating layer of atactic polystyrene (PS, MW=3350, used as received from commercial sources) was deposited from toluene solution (1% wt) by spin-coating (3000 rpm, 1000 rpm s^{-1}, 30 s). The resulting layer had a thickness of 30 ± 2 nm as measured by scratching the surface and measuring the step by profilometry. The PS layer was imaged by AFM and found to be smooth with RMS surface roughness of 0.05 nm over an area of 500×500 nm (Figure S4). Thin films of the compounds **1-4** were evaporated in vacuum (1×10^{-7} mbar) onto the PS-coated substrates, the temperatures to keep a rate of 0.2 Å s^{-1} were: *T*(**1**)=165 ºC, *T*(**2**)=125 ºC, *T*(**3**)= 180 ºC and *T*(**4**)=150 ºC, to finally reach thicknesses of 50 nm. The OFET structures were finished by evaporating MoO_3 followed by Au through a shadow mask at a rate of 0.1 Å s^{-1} and 0.2 Å s^{-1} respectively, with thicknesses of 8 nm and 25 nm respectively as measured by profilometry. The OFET channels had 2 mm width and 40-140 μm length. The channel lengths were confirmed by profilometry. The current-voltage characteristics were measured with a Keithley 2636A semiconductor parameter analyzer at room temperature under ambient atmosphere. The field-effect mobility was extracted in the saturation regime by Equation 1:

$$\mu = \left(\frac{d\sqrt{I_{SD}}}{dV_{SG}}\right)^2 \frac{2L}{WC_i} \qquad (1)$$

where μ is the field-effect mobility in the saturation regime, I_{SD} is the source-drain current, V_{SG} is the source-gate voltage, L is the channel length, W is the channel width, and C_i is the gate capacitance per unit area. The polystyrene layer acts as an additional insulator in series with the SiO_2, and thus the total series capacitance C_i was calculated by Equation 2:

$$C_i = \frac{C_1 C_2}{C_1 + C_2} \qquad (2)$$

where C_1 and C_2 are the capacitances per unit area of the SiO_2 and PS layers,

$$C = \frac{A\varepsilon_0\varepsilon_r}{d} \qquad (3)$$

where A is the area, ε_0 is the vacuum permittivity, ε_r is the relative permittivity of the insulator, and d is the thickness of the insulator. For a 300 nm layer of SiO_2 (ε_r=3.9) in series with a 30 nm layer of PS (ε_r=2.4), the total capacitance is C_i=9.9 nF cm^{-2}. It is noted that if the polystyrene layer is not considered as an additional insulator in series with the SiO_2, the capacitance per unit area would be 11.5 nF cm^{-2} and the mobility would be underestimated by a factor of 1.16.

Computational details: The theoretical treatment of the molecules was based on density functional theory (DFT) methods at B3LYP/6-311++G(d,p) level[20] as implemented in Jaguar.[21],[22] The reorganization energy (λ) was first computed by optimizing the molecular structure both in its neutral and charged state. The reorganization energy, combined with data of the X-ray structure, was subsequently used to calculate the transfer integrals (t_{ab}) at the same DFT level. In our case, the CDFT formulation reported by Wu and van Voorhis[23] has been used as implemented in the Material Science Suite of Schrödinger.[24] Transfer integrals were computed for a model built from the X-ray diffraction data with a molecule surrounded by a set of molecules in van der Waals contact. The graphical processing of the computational calculations was done with Maestro 2017-4.[25]

RESULTS AND DISCUSION

The electronic structure of carbazolocarbazoles was determined by UV-vis spectroscopy and cyclic voltammetry. The absorption spectra of compounds **1** to **4** (Figure 2) show that their different geometry translates into a different vibrational structure as evidenced by the location of the α, p and β bands typically observed in fused polyaromatic systems according to Clar's definition.[26] Moreover, whereas the lowest energy band of compound **1** appears at 380 nm, the same band in isomer **3** is bathochromically shifted at 405 nm. Despite the similarities between these polyheteroaromatic molecules their different geometries results in a small narrowing of the optical bandgap for isomer **3**. As far as the effect of alkyl chains is concerned, this subtly manifests in compounds **2** and **4** as a red shift in the absorption bands with respect to the unsubstituted carbazolocarbazoles. As expected, the UV-vis spectra of thin films show a bathochromic displacement of the absorption bands resulting from the intermolecular interactions in the solid state. This effect is a bit more perceptible for the carbazolo[2,1-*a*]carbazole derivatives **1** and **2**. In agreement with these results, since the optical gap can be related to the HOMO-LUMO gap, the isomerism of compounds **1**-**4** only has a slight influence on the electronic structure (Table 1). In general, carbazolocarbazoles present a relatively wide energy gap that corresponds to materials virtually transparent to the visible light.

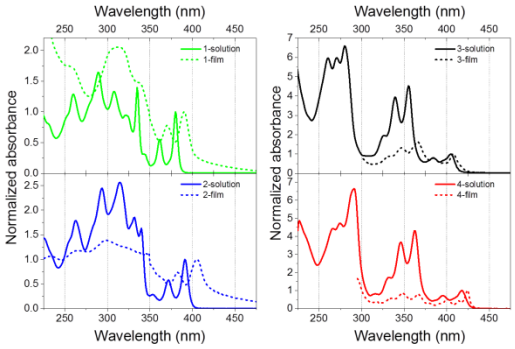

Figure 2. Absorption spectra of compounds **1**-**4** in THF solution (10^{-5} M) and thin film.

Concerning the electrochemical characterization (Figure S3), cyclic voltammetry experiments were performed both in solution and thin films. These latter results from solid state samples were employed for the assessment of the electronic structure as it corresponds to the materials that will be used for the OFETs fabrication afterwards. In general, quasi-reversible and irreversible cyclic voltammograms were obtained for the series of carbazolocarbazoles. Focusing on the onset of the first oxidation wave carbazolo[2,1-*a*]carbazole, **1**, showed a potential of 0.95 V, with its *N,N'*-dioctyl derivative, **2**, displaying a detectable increase of the current at 0.86 V. Analogously, the onset of the carbazolo[4,3-*c*]carbazole, **3**, and its dialkyl derivative **4**, were also very similar, with potentials of 0.83 V and 0.91 V, respectively. From these results we can consider that the effect of *N*-alkyl chains on the electronic structure of the carbazolocarbazoles is practically negligible. Analogously, the differences between the oxidation potentials of the isomers are neither significant. This can be justified by the Clar's rules of polyaromatic hydrocarbons. Both hexacyclic systems have a benzenoid character and, according to the Clar's rule, three sextets can be drawn in both cases. Besides, each isomer can be represented by two Clar structures with the maximum number of sextets.[27] Thus, considering the correlation between the ionization potentials and the number of Clar structures in the fused polyheteroaromatic molecules, this would explain the similar redox potentials.

The HOMO energies were estimated from the onset of the first oxidation wave using the ferrocene onset potential (0.44 V) as a reference to set the energy with respect to the vacuum level.[28] As expected, very similar values were

obtained for compounds **1**-**4** revealing that for these particular isomers the different geometry of the catacondensation does not significantly affect the orbital energy. Thus, the low HOMO energies confer stability towards ambient oxidation on the carbazolocarbazoles. In combination with the HOMO-LUMO gap, previously determined from the absorption spectra, the LUMO energy can be estimated by difference.

Table 1. Optical and electrochemical properties of carbazolocarbazoles **1**-**4**.

	$\lambda_{abs.,soln.}$ (nm)[a]	$\lambda_{abs.,film}$ (nm)[a]	$E_g^{opt,soln.}$ (eV)[b]	$E_g^{opt,film}$ (eV)[b]	E_{HOMO} (eV)[c]	E_{LUMO} (eV)[d]
1	380	390	3.22	3.08	-5.31	-2.23
2	391	405	3.11	2.95	-5.22	-2.27
3	405	408	3.02	2.93	-5.19	-2.26
4	418	424	2.97	2.88	-5.27	-2.39

[a] Higher absorption band wavelength; [b] Optical energy gap determined from the onset of the higher absorption band; [c] $E_{HOMO} \approx -(E_{onset} - E_{onset\ Fc/Fc+}) - 4.8$; [d] $|E_g| \approx |E_{HOMO} - E_{LUMO}|$.

In agreement with the characterization of their electronic structure, carbazolocarbazoles are suitable for their evaluation as hole transporting materials. Accordingly, to further investigate the electronic properties the reported azaphenacenes, they were used as semiconductors in thin film OFETs with a bottom-gate, top-contact architecture. Bearing in mind the variables that can affect the device performance, the interfacial regions of the transistor become critical due to their influence on the semiconductor morphology,[12] in the case of the semiconductor-dielectric interface, and also on the contact resistance,[29] in the case of the semiconductor-electrode interface. As far as the studies about carbazolocarbazoles are concerned, some of these compounds have been previously characterized using HMDS (hexamethyldisilazane) self-assembled monolayers for the functionalization of the silicon dioxide interface.[35] Moreover, we have also investigated the use of different k gate dielectrics such as silicon dioxide and zirconium dioxide, coated in this case with a parylene thin film, and the incorporation of F_4TCNQ (2,3,5,6-tetrafluoro-7,7,8,8-tetracyanoquinodimethane) as an interfacial layer for the top contacts.[37] In our exploration of the fabrication conditions we have now optimized the dielectric layer by coating the surface of the silicon dioxide with polystyrene. This polymer forms very homogeneous and flat films using straightforward solution processing. Besides, its low relative permittivity (ε_r=2.4) contributes to the reduction of the dipolar energetic disorder at the interface[30] and consequently this could improve the field-effect mobility.[31]As far as the semiconductor-electrode interface is concerned, MoO_3/Au contacts were used. Considering the low lying HOMO of carbazolocarbazoles the interfacial layer of molybdenum oxide, with a high work function (5.9 eV), should favor the formation of ohmic contacts.[32] All the reported transistors were characterized in air. The output curves (Figure 3) exhibit linear *I*-*V* characteristics at low source-drain voltages which indicate that no significant contact resistance is present as it was intended by using the interfacial layer of MoO_3. The parameters extracted from the OFETs *I*-*V* transfer characteristics are summarized in Table 2. At this point, it is worth highlighting the high mobility of 1.3 $cm^2\ V^{-1}\ s^{-1}$ measured for compound **1**, which contrasts to the other carbazolocarbazoles and emphasizes the effect of the molecular structure. The unsubstituted isomers **1** and **3** show a noticeable difference of almost four orders of magnitude in their mobilities. Concerning the attachment of octyl chains to the nitrogen atoms, it has opposite effects, leading to a lower mobility in the case of carbazolo[2,1-*a*]carbazole derivative **2** and to a better charge transport in the case of compound **4**. Nevertheless, it is interesting to check how *N*-alkylation seems to compensate the effect of the aromatic core isomerism since the mobilities of compounds **2** and **4** differ in a little more than one order of magnitude only. The mobility reached by compound **1** represents the best value reported within the family of pyrrole-based polyheteroaromatic systems,[37-43] approaching a single crystal-like performance in similar azaphenacenes[33] and becoming comparable to the hole mobility reported for pentacene in analogous thin film OFETs,[34] in terms of architecture and processing conditions.

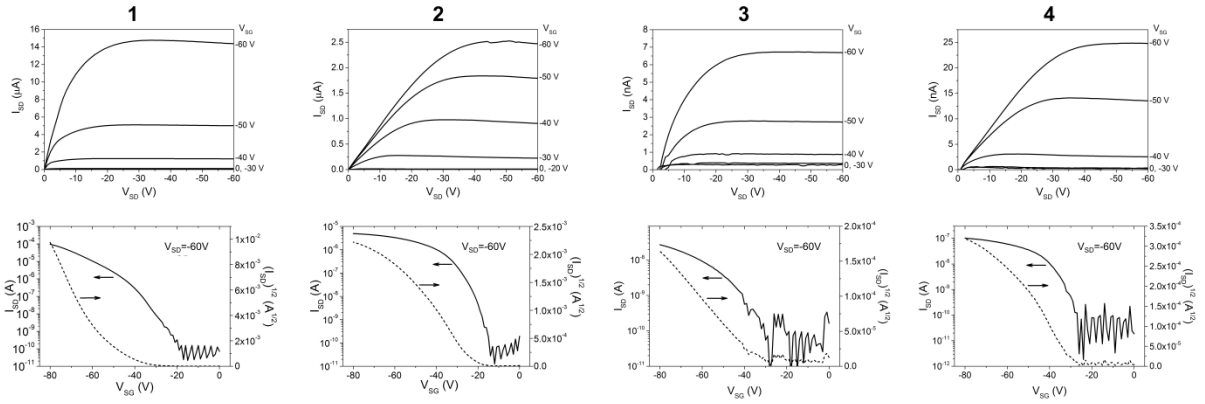

Figure 3. Output (top row) and transfer (bottom row) characteristics of thin film OFETs.

Table 2. Thin film OFETs parameters.

	$\mu_{max.}$ ($cm^2V^{-1}s^{-1}$)	$\mu_{avg.}$ ($cm^2V^{-1}s^{-1}$)[a]	V_{on} (V)	I_{on}/I_{off}
1	1.3	1.0 ± 0.2	-20	10^6
2	6×10^{-2}	$5\times10^{-2} \pm 8\times10^{-3}$	-17	10^5
3	5×10^{-4}	$4.5\times10^{-4} \pm 4\times10^{-5}$	-28	10^3
4	2×10^{-3}	$10^{-3} \pm 8\times10^{-4}$	-26	10^4

[a] Average values calculated from the characterization of six devices.

With the aim of getting a better understanding of the origin of this high mobility and its connection with the structure of the carbazolocarbazole isomers (**1** and **3**) and their *N*-alky derivatives (**2** and **4**), the solid state packing was analyzed in detail (Figure 4 and Table 3). Crystal structures of compounds **1**-**4** were obtained by single crystal X-ray diffraction. The fused hexacyclic system remained flat for the four molecules which crystalized in a monoclinic cell. However, the different geometry of the carbazolocarbazole isomers manifests in the different lengths (12.6 Å *vs.* 12.1 Å) and widths (3.7 Å *vs.* 4.3 Å) of the carbazolo[2,1-*a*]carbazole, **1**, and carbazolo[4,3-*c*]carbazole, **3**, cores respectively. Regarding the *N*-alkylated molecules, dissimilar orientations of the alkyl groups were observed (Figure 4a). Whereas side chains in compound **2** formed 145º angle with the aromatic core, the orientation of the chains in compound **4** were almost orthogonal to the plane of the aromatic system.

Figure 4. X-ray diffraction structures. a) Molecular packing projection across the long axis; b) Molecular packing projection across the short axis; c) Simplified view of molecules showing face-to-face π-π stacking. Hydrogen atoms have been omitted for the sake of clarity. Dotted lines are included to locate the centroids.

Table 3. Crystal packing of carbazolocarbazoles **1**-**4**.

		1	**2**	**3**	**4**
Conjugated core size[a]	Length (Å)	12.6		12.1	
	Width (Å)	3.7		4.3	
Intermolecular face-to-face interactions	π-π stacking distance (Å)	3.2	3.4	3.3	3.2
	Short axis slippage (Å) [b]	3.8	3.0	4.0	5.7
	Long axis slippage	0.1	0.5	1.0	5.1
Intermolecular edge-to-face interactions[b]	Edge-to-face distance (Å) [a]	3.5	3.6	3.4[c]	3.6
	Long axis slippage (Å) [b]	1.7	7.1	6.9; 7.6	1.5
	Crystal density (g/cm^3)	1.416	1.187	1.396	1.119
	d spacing (Å)	14.4	17.9	8.9	15.2
	Conjugated core inclination in thin film (º)[d]	11	29	31	35

[a] Due to the possible uncertainty in hydrogen atoms location, data are given as carbon-carbon distances; [b] Distance between centroids; [c] nitrogen-nitrogen distance; [d] Tentative estimation of the angle with the normal to the substrate.

Since crystal packing defines the intermolecular contacts in the solid state, which ultimately determine the electronic coupling related to the charge transfer, a comparative study of the carbazolocarbazoles packing provides a more detailed justification of the measured mobilities. The projection of the crystal packing across the long axis of the π-conjugated core for the molecules in van der Waals contact revealed that all of them adopted a herringbone arrangement (Figure 4a). Excepting the case of compound **3**, where each molecule is in contact with ten more surrounding molecules, the rest of the studied carbazolocarbazoles displayed the typical pattern with each molecule having van der Waals contact with six neighbor molecules. Nevertheless, it is interesting to realize the different intermolecular interactions in the solid state structures. Regarding the π-π stacking, the distance between molecules establishing face-to-face interactions spanned between 3.2 Å and 3.4 Å. More importantly, noticeable differences were observed in the intermolecular slippage calculated from the distance between centroids (Table 3). Looking at the molecules packed in parallel planes (Figure 4c), transversal and longitudinal shifts, along the short and long molecular axis respectively, are shorter for compounds, **1** and **2**, than for the corresponding isomers, **3** and **4**. However, in the case of the unsubstituted molecules, **1** and **3**, the different geometry still allows certain intermolecular overlap in the case of carbazolo[4,3-*c*]carbazole, **3**. Conversely, when *N*-alkylated molecules are compared, the different orientation of the side chains motivates a better overlap in the carbazolo[2,1-*a*]carbazole derivative, **2**, than in the isomer **4**. When analyzing the features of the herringbone packing, it is also important to look at the edge-to-face interactions that can be better studied through the projection of the packing across the short molecular axis (Figure 4b). Although the minimum edge-to-face distances were almost the same in all cases, significant differences were observed in the relative intermolecular shifts, especially along the long axis (Table 3), with compounds **1** and **4** showing much shorter displacements than **2** and **3**. Overall, it can be concluded that the more compact packing of compound **1**, determined by short longitudinal shifts either for molecules establishing face-to-face or edge-to-face interactions, seems to correlate well with the above described charge mobility trend.

Out-of-plane X-ray diffraction experiments were done on the semiconducting thin films proving their crystallinity (Figure 5). Additionally, the detection of a periodic series of the peaks corroborated that the films were constituted by a single crystal phase. The comparison of these results with the simulated powder diffractogram obtained from the

single crystal data, showed the coincidence of the 2θ angle for the main peaks proving that the molecular arrangement in the film is coincident with that observed in the single crystal.

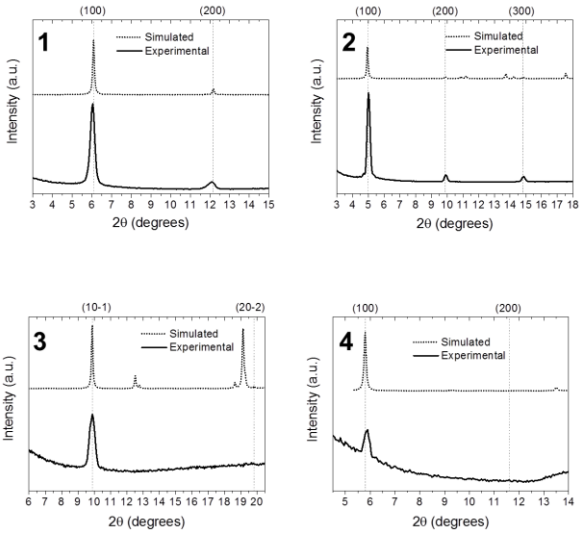

Figure 5. X-ray diffractograms of carbazolocarbazole thin films.

Thus, the indexation of the peaks enabled an approximate description of the molecular disposition in the thin film (Figure 6). Accordingly, carbazolocarbazoles tend to adopt an edge-on orientation vertically standing on their short edge. Compounds **1** and **3**, respectively oriented with the (100) and (10$\bar{1}$) planes parallel to the substrate surface, would define a lamellar structure. The d spacing, determined from the distance between (h00) crystallographic planes, is in good agreement with the length of compound **1**, but this is not observed when interplanar distances are measured for the (h0$\bar{1}$) planes of compound **3**. This indicates that molecules adopt a different inclination with respect to the normal to the substrate. Thus, whereas **1** formed an angle of 11º only, compound **3** was more tilted, forming an angle of 31º. For molecules packed with similar intermolecular distances, the inclination of the molecules, along with the longitudinal slippage, determines the extension of the intermolecular interactions through the long molecular axis.[6, 35] Therefore, the more vertical arrangement of carbazolo[2,1-*a*]carbazole, **1**, reinforced by the previously mentioned compact packing, results in a denser 2D lamellar structure.

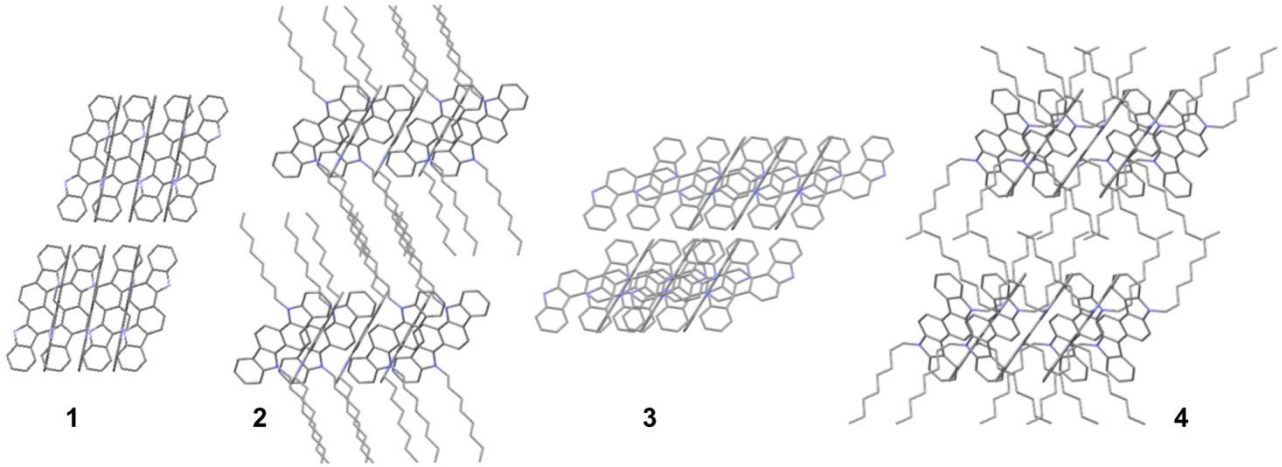

Figure 6. Idealized view of the carbazolocarbazoles lamellar packing in thin films.

The *N*-alkylated derivatives, **2** and **4**, also formed crystalline thin films with a regular packing defined by the (h00) planes in both cases. As expected, in this case the disposition of the molecules was conditioned by the orientation of

the alkyl chains. Compound **2** packed with a stratified structure where the alkyl chains were interdigitated. Conversely, no interaction between the side chains was observed in compound **4**. Nevertheless, despite the dissimilar packing of the alkyl chains, the inclination of the aromatic cores with respect to the normal to the substrate remained approximately within the same range (29º for compound **2** and 35º for compound **4**).

As stated by the electron transfer theory, the electronic coupling and the reorganization energy are the parameters that mainly determine the charge transfer rate in molecular materials.[36] Therefore transfer integrals between couples of molecules having face-to-face or edge-to-face interactions were calculated by DFT methods using the crystal packing as a model for the molecular arrangement. As it can be observed in Figure 7, the transfer integrals between stacked molecules ($t_{1\text{-}2}$ and $t_{1\text{-}3}$) show a good correlation with the above discussed relative intermolecular slippage and the degree of π-surface overlap (Figure 4c). Accordingly, higher transfer integrals are obtained for compounds **2** and **3** where certain overlap was observed between the molecules packed through face-to-face interactions. Although compound **1** did not show this kind of intermolecular intersection, its moderate transversal and short longitudinal shifts still enable a noticeable orbital interaction. An analogous effect of the intermolecular shift was verified for the transfer integrals calculated between molecules packed in an edge-to-face fashion. Focusing on the unsubstituted carbazolocarbazoles, compound **3** shows two different sets of interactions for the couples labeled as $t_{1\text{-}4}$, $t_{1\text{-}6}$, $t_{1\text{-}8}$, $t_{1\text{-}10}$ and the couples $t_{1\text{-}5}$, $t_{1\text{-}7}$, $t_{1\text{-}9}$, $t_{1\text{-}11}$ that match well the two longitudinal shifts previously shown (Figure 4b and Table 3), with a shorter slippage for the second group of couples. Interestingly, the transfer integral measured between molecules of carbazolocarbazole **1** having edge-to-face interactions are larger due to the little intermolecular slippage. Then, the values of the transfer integrals in the different directions defined by the molecular packing show that for compound **3** charge transport should preferentially occur along the stacking direction resulting in an anisotropic transport. Nevertheless, despite the lower transfer integral of compound **1** along the stacking direction, the transfer integrals between molecules interacting edge-to-face have similar values to those of molecules having face-to-face interactions, which defines an almost isotropic 2D transport environment benefiting the charge mobility in polycrystalline thin films. Additionally, the internal reorganization energy, which accounts for the energy difference due to the structural changes between the neutral and charged states in a charge transfer process,[36b, 37] shows a lower value for carbazolocarbazole **1**, meaning that this isomer can better adapt to the structural transition occurring during charge hopping. In agreement with these results, the compact lamellar packing previously described for compound **1**, benefits the isotropy for the charge transport and shows good correlation with the high mobility measured.[38]

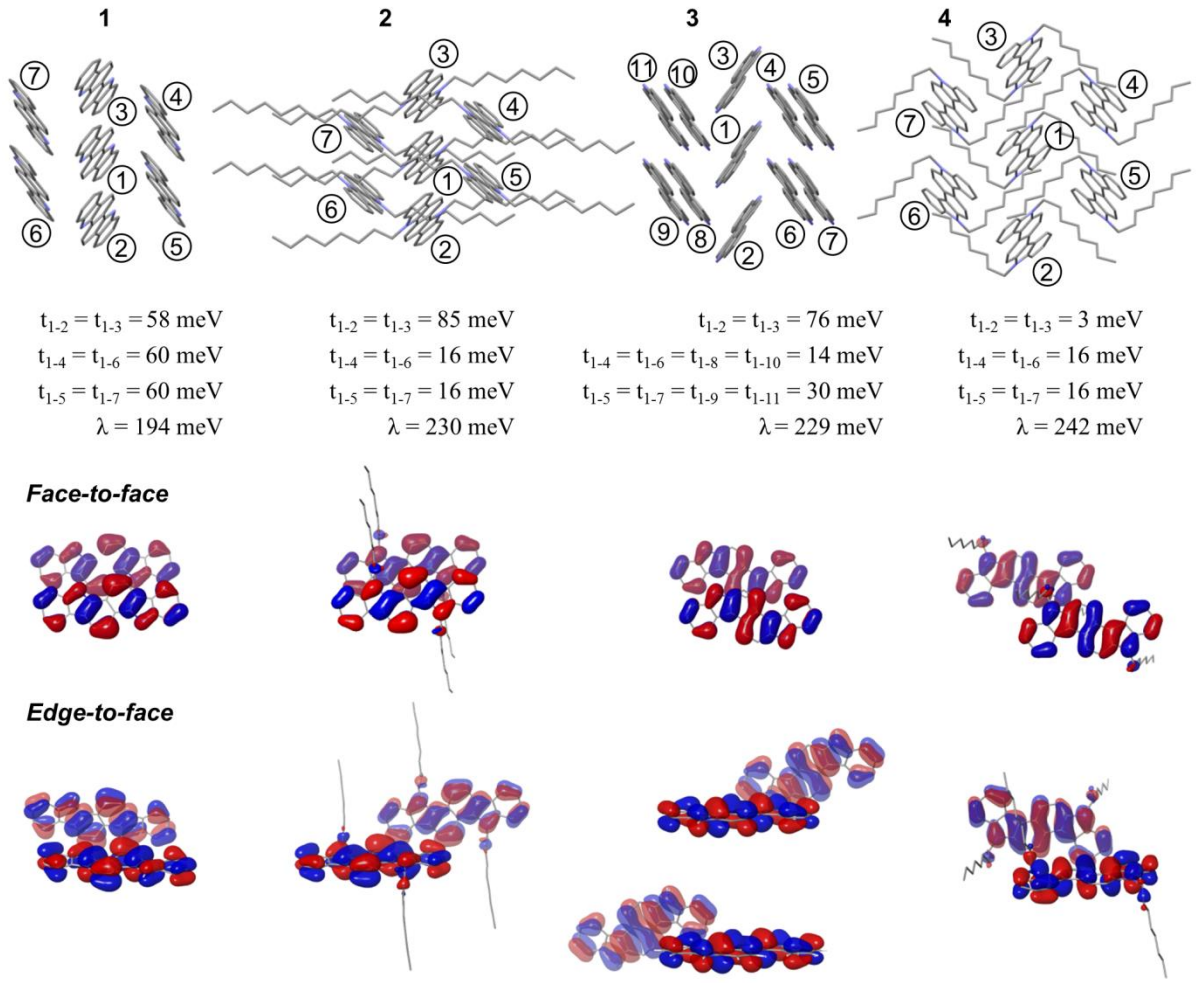

Figure 7. Charge transport parameters calculated for carbazolocarbazoles **1**-**4**. HOMO isosurfaces in molecules establishing face-to-face and edge-to-face interactions.

The transfer integrals calculated for the *N,N'*-dioctylcarbazolocarbazoles, **2** and **4**, show quite different values along the stacking direction, as it could be expected from the intermolecular displacements that significantly reduce the face-to-face orbital overlap for compound **4**. In contrast, the edge-to-face interactions lead to similar transfer integrals for both compounds **2** and **4**. Again, this would define an anisotropic 2D charge transport within the lamellar arrangement where, as expected, the better mobility measured for the molecule **2** presumably correlates with its higher transfer integrals along the stacking direction.

Since the morphology of organic semiconductors can also critically condition their charge transport properties, we additionally studied the thin film morphology of the semiconducting layer in the previously described OFETs. The AFM images evidenced a remarkable influence of the alkyl chains in the morphology of carbazolocarbazoles deposited on SiO_2-polystyrene (Figure 8).[39] Whereas plain carbazolocarbazoles **1** and **3** showed a granular appearance, the attachment of alkyl chains caused an increase in the grain size. Although larger grain size is a desirable feature, it has been observed that the connectivity between grains becomes an even more important aspect for improving charge transport in thin films.[40] Interestingly, the different disposition of the *N*-alkyl chains in **2** and **4** leads to clear differences in their morphology. As far as compound **2** is concerned, it forms regular rod-like domains. Nevertheless, carbazolocarbazole **4** takes more irregular shapes. This particular result also manifests in the root mean squared roughness that shows a softer surface for the thin films of compounds **1**-**3** (r_{rms-1}= 5.7 nm; r_{rms-2}= 4.3 nm; r_{rms-3}= 3.7 nm) than **4** (r_{rms-4}= 13.8 nm).

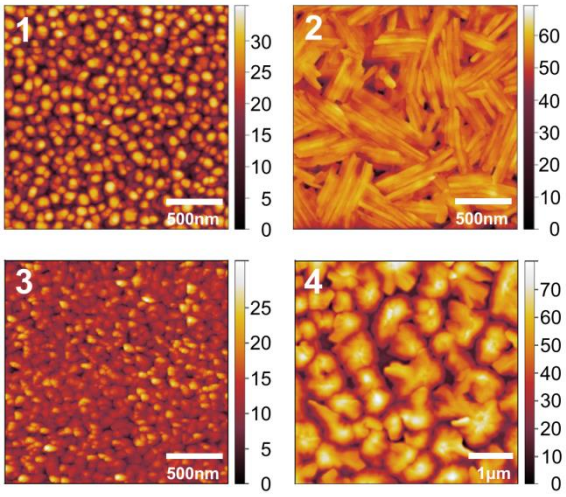

Figure 8. AFM images of carbazolocarbazoles **1-4** thin films on SiO_2-polystyrene.

Thus, the good uniformity of grain sizes, in conjunction with a suitable grain connection, film coverage and softness are the morphological features found in carbazolocarbazole **1** which, along with the compact crystal packing and the isotropy observed in its dense lamellar arrangement constitute the features dictated by the molecular structure that correlate with a very good charge transport in thin film OFETs.

CONCLUSIONS

In summary, a comparative study of carbazolocarbazole isomers has confirmed the potential of these azaphenacenes to be applied as organic semiconductors. Particularly, the mobility determined for carbazolo[2,1-*a*]carbazole breaks the barrier of 1 $cm^2V^{-1}s^{-1}$ in pyrrole-based polyheteroaromatic systems, reaching an outstanding hole mobility of 1.3 $cm^2V^{-1}s^{-1}$ within the family of azaphenacenes in thin film OFETs. The interfacial optimization, using polystyrene as part of the dielectric bilayer and molybdenum oxide to reduce contact resistance, has revealed as the appropriate combination for OFET fabrication without any thermal treatment. Moreover, the good charge transport in thin film transistors results from the adequacy of the crystal packing and thin film morphology favored by the geometry of this fused hexacyclic system. The short intermolecular longitudinal slippage represents a key structural parameter leading to a compact packing that seems to be conserved in the thin film. Densely packed molecules adopt a lamellar structure where the aromatic core presumably deposits following an edge-on disposition with a minimum vertical deviation. The 2D compact arrangement favors orbital overlap and defines an almost isotropic 2D charge transport environment. All these structural properties are reinforced by a homogeneous and soft granular thin film morphology that contributes to the observed good charge transport.

ASSOCIATED CONTENT

Supporting Information. NMR spectra, thermal characterization, cyclic voltammetry, polystyrene AFM and stability of transfer characteristics.

AUTHOR INFORMATION

Corresponding Author

*E-mail: davidcc@um.es

David Curiel: ORCID number 0000-0002-6717-6305

Present Addresses

‖Molecular Materials and Nanosystems, Institute for Complex Molecular Systems, Eindhoven University of Technology, P.O. Box 513, 5600 MB Eindhoven, The Netherlands.

Funding Sources

Ministry of Economy and Competitiveness; Fundación Séneca

Notes

Authors declare no conflict of interest.

ACKNOWLEDGEMENTS

Authors are grateful for the financial support from the Spanish Ministry of Economy and Competitiveness (CTQ2014-58875) and (CTQ2015-67927-R).

REFERENCES

[1] a) R.-P. Xu, Y.-Q. Li, J.-X. Tang, *J. Mater. Chem. C* **2016**, *4*, 9116-9142; b) B. H. Lee, B. B. Y. Hsu, S. N. Patel, J. Labram, C. Luo, G. C. Bazan, A. J. Heeger, *Nano Lett.* **2016**, *16*, 314-319; c) Q. Lin, H. Huang, Y. Jing, H. Fu, P. Chang, D. Li, Y. Yao, Z. Fan, *J. Mater. Chem. C* **2014**, *2*, 1233-1247; d) B. Kang, W. H. Lee, K. Cho, *ACS Appl. Mater. Interfaces* **2013**, *5*, 2302-2315.

[2] For a monographic issue on flexible and stretchable devices see: Adv. Mater. 2016, 28, 4165-4562.

[3] For a monographic issue on materials for organic electronics see: J. Mater. Chem. C, 2016, 7, 3665-3874.

[4] a) Q. Ye, C. Chi, *Chem. Mater.* **2014**, *26*, 4046-4056; b) J. Mei, Y. Diao, A. L. Appleton, L. Fang, Z. Bao, *J. Am. Chem. Soc.* **2013**, *135*, 6724-6746; c) W. Jiang, Y. Li, Z. Wang, *Chem. Soc. Rev.* **2013**, *42*, 6113-6127; d) K. Takimiya, S. Shinamura, I. Osaka, E. Miyazaki, *Adv. Mater.* **2011**, *23*, 4347-4370; eJ. E. Anthony, *Chem. Rev.* **2006**, *106*, 5028-5048.

[5] a) J. L. Brédas, J. P. Calbert, D. A. da Silva Filho, J. Cornil, *Proc. Natl. Acad. Sci.* **2002**, *99*, 5804-5809; b) Y. Olivier, V. Lemaur, J. L. Brédas, J. Cornil, *J. Phys. Chem. A* **2006**, *110*, 6356-6364.

[6] A. O. F. Jones, B. Chattopadhyay, Y. H. Geerts, R. Resel, *Adv. Funct. Mater.* **2016**, *26*, 2233-2255.

[7] a) C. Mitsui, T. Okamoto, H. Matsui, M. Yamagishi, T. Matsushita, J. Soeda, K. Miwa, H. Sato, A. Yamano, T. Uemura, J. Takeya, *Chem. Mater.* **2013**, *25*, 3952-3956; b) M. Nakano, H. Mori, S. Shinamura, K. Takimiya, *Chem. Mater.* **2012**, *24*, 190-198; c) M. Nakano, K. Niimi, E. Miyazaki, I. Osaka, K. Takimiya, *J. Org. Chem.* **2012**, *77*, 8099-8111; d) L. Yan, Y. Zhao, H. Yu, Z. Hu, Y. He, A. Li, O. Goto, C. Yan, T. Chen, R. Chen, Y.-L. Loo, D. F. Perepichka, H. Meng, W. Huang, *J. Mater. Chem. C* **2016**, *4*, 3517-3522.

[8] a) H. Mori, X.-c. Chen, N.-h. Chang, S. Hamao, Y. Kubozono, K. Nakajima, Y. Nishihara, *J. Org. Chem.* **2014**, *79*, 4973-4983; b) Y. Tsutsui, G. Schweicher, B. Chattopadhyay, T. Sakurai, J.-B. Arlin, C. Ruzié, A. Aliev, A. Ciesielski, S. Colella, A. R. Kennedy, V. Lemaur, Y. Olivier, R. Hadji, L. Sanguinet, F. Castet, S. Osella, D. Dudenko, D. Beljonne, J. Cornil, P. Samorì, S. Seki, Y. H. Geerts, *Adv. Mater.* **2016**, *28*, 7106-7114; cC. Wang, H. Nakamura, H. Sugino, K. Takimiya, *Chem. Commun.* **2017**, *53*, 9594-9597.

[9] C. Wang, H. Dong, L. Jiang, W. Hu, *Chem. Soc. Rev.* **2018**.

[10] a) Y. Wen, Y. Liu, Y. Guo, G. Yu, W. Hu, *Chem. Rev.* **2011**, *111*, 3358-3406; b) S. Liu, W. M. Wang, A. L. Briseno, S. C. B. Mannsfeld, Z. Bao, *Adv. Mater.* **2009**, *21*, 1217-1232.

[11] a) S. Casalini, C. A. Bortolotti, F. Leonardi, F. Biscarini, *Chem. Soc. Rev.* **2017**, *46*, 40-71; b) Y. Li, H. Wang, Z. Shi, J. Mei, X. Wang, D. Yan, Z. Cui, *Polymer Chemistry* **2015**, *6*, 6651-6658.

[12] A. A. Virkar, S. Mannsfeld, Z. Bao, N. Stingelin, *Adv. Mater.* **2010**, *22*, 3857-3875.

[13] a) Ş. Atahan-Evrenk, A. Aspuru-Guzik, in *Prediction and Calculation of Crystal Structures: Methods and Applications* (Eds.: S. Atahan-Evrenk, A. Aspuru-Guzik), Springer International Publishing, Cham, **2014**, pp. 95-138; b) S. M. Ryno, C. Risko, J.-L. Brédas, *J. Am. Chem. Soc.* **2014**, *136*, 6421-6427; c) S. M. Ryno, C. Risko, J.-L. Brédas, *ACS Appl. Mater. Interfaces* **2016**, *8*, 14053-14062; d) I. Yavuz, B. N. Martin, J. Park, K. N. Houk, *J. Am. Chem. Soc.* **2015**, *137*, 2856-2866.

[14] H. Dong, X. Fu, J. Liu, Z. Wang, W. Hu, *Adv. Mater.* **2013**, *25*, 6158-6183.

[15] a) D. Curiel, M. Más-Montoya, A. Uruvakili, R. A. Orenes, H. Pallamreddy, P. Molina, *Org. Lett.* **2010**, *12*, 3164-3167; b) D. Curiel, M. Mas-Montoya, C.-H. Chang, P.-Y. Chen, C.-W. Tai, A. Tarraga, *J. Mater. Chem.*

C **2013**, *1*, 3421-3429; c) M. Mas-Montoya, R. P. Ortiz, D. Curiel, A. Espinosa, M. Allain, A. Facchetti, T. J. Marks, *J. Mater. Chem. C* **2013**, *1*, 1959-1969; d) D. Curiel, M. M. Montoya, M. Hummert, M. Riede, K. Leo, *Org. Electron.* **2015**, *17*, 28-32; e) M. Mas-Montoya, J. P. Ceron-Carrasco, S. Hamao, R. Eguchi, Y. Kubozono, A. Tarraga, D. Curiel, *J. Mater. Chem. C* **2017**, *5*, 7020-7027.

[16] a) K. J. Thorley, C. Risko, *J. Mater. Chem. C* **2016**, *4*, 4040-4048; b) I. Osaka, S. Shinamura, T. Abe, K. Takimiya, *J. Mater. Chem. C* **2013**, *1*, 1297-1304; c) M. Nakano, S. Shinamura, Y. Houchin, I. Osaka, E. Miyazaki, K. Takimiya, *Chem. Commun.* **2012**, *48*, 5671-5673; d) S. Shinamura, I. Osaka, E. Miyazaki, A. Nakao, M. Yamagishi, J. Takeya, K. Takimiya, *J. Am. Chem. Soc.* **2011**, *133*, 5024-5035.

[17] a) K. Ivaniuk, V. Cherpak, P. Stakhira, Z. Hotra, B. Minaev, G. Baryshnikov, E. Stromylo, D. Volyniuk, J. V. Grazulevicius, A. Lazauskas, S. Tamulevicius, B. Witulski, M. E. Light, P. Gawrys, R. J. Whitby, G. Wiosna-Salyga, B. Luszczynska, *J. Phys. Chem. C* **2016**, *120*, 6206-6217; b) I. Cho, S. K. Park, B. Kang, J. W. Chung, J. H. Kim, K. Cho, S. Y. Park, *Adv. Funct. Mater.* **2016**, *26*, 2966-2973; c) G. V. Baryshnikov, P. Gawrys, K. Ivaniuk, B. Witulski, R. J. Whitby, A. Al-Muhammad, B. Minaev, V. Cherpak, P. Stakhira, D. Volyniuk, G. Wiosna-Salyga, B. Luszczynska, A. Lazauskas, S. Tamulevicius, J. V. Grazulevicius, *J. Mater. Chem. C* **2016**, *4*, 5795-5805; d) J. H. Park, H. S. Lee, S. Park, S.-W. Min, Y. Yi, C.-G. Cho, J. Han, T. W. Kim, S. Im, *Adv. Funct. Mater.* **2014**, *24*, 1109-1116; e) T. V. Pho, J. D. Yuen, J. A. Kurzman, B. G. Smith, M. Miao, W. T. Walker, R. Seshadri, F. Wudl, *J. Am. Chem. Soc.* **2012**, *134*, 18185-18188; f) P.-L. T. Boudreault, S. Wakim, N. Blouin, M. Simard, C. Tessier, Y. Tao, M. Leclerc, *J. Am. Chem. Soc.* **2007**, *129*, 9125-9136; g) Y. Wu, Y. Li, S. Gardner, B. S. Ong, *J. Am. Chem. Soc.* **2005**, *127*, 614-618.

[18] a) U. H. F. Bunz, *Acc. Chem. Res.* **2015**, *48*, 1676-1686; b) Q. Miao, *Adv. Mater.* **2014**, *26*, 5541-5549; cU. H. F. Bunz, *Chemistry--A European Journal* **2009**, *15*, 6780-6789.

[19] M. Randić, *Chem. Rev.* **2003**, *103*, 3449-3606.

[20] M. Randić, *Chem. Phys. Lett.* **2014**, *601*, 1-5.

[21] A. D. Bochevarov, E. Harder, T. F. Hughes, J. R. Greenwood, D. A. Braden, D. M. Philipp, D. Rinaldo, M. D. Halls, J. Zhang, R. A. Friesner, *Int. J. Quantum Chem.* **2013**, *113*, 2110-2142.

[22] Schrödinger Release 2016-4: Jaguar, Schrödinger, LLC, New York, NY, 2016.

[23] Q. Wu, T. Van Voorhis, *Phys. Rev. A* **2005**, *72*, 024502.

[24] Materials Science Suite 2016-4, Schrödinger, LLC, New York, NY, 2016.

[25] Schrödinger Release 2016-4: Maestro, v., Schrödinger, LLC, New York, NY, 2016.

[26] E. Clar, *The Aromatic Sextet*, Wiley-Interscience, **1972**.

[27] E. Clar, W. Schmidt, *Tetrahedron* **1975**, *31*, 2263-2271.

[28] a) R. O. Loutfy, *J. Chem. Phys.* **1977**, *66*, 4781-4787; b) R. Cernini, X. C. Li, G. W. C. Spencer, A. B. Holmes, S. C. Moratti, R. H. Friend, *Synth. Met.* **1997**, *84*, 359-360; c) Z.-F. Yao, J.-Y. Wang, J. Pei, *Cryst. Growth Des.* **2018**, *18*, 7-15.

[29] S. Choi, C. Fuentes-Hernandez, C.-Y. Wang, T. M. Khan, F. A. Larrain, Y. Zhang, S. Barlow, S. R. Marder, B. Kippelen, *ACS Appl. Mater. Interfaces* **2016**, *8*, 24744-24752.

[30] a) A. F. Stassen, R. W. I. d. Boer, N. N. Iosad, A. F. Morpurgo, *Appl. Phys. Lett.* **2004**, *85*, 3899-3901; b) H. S. Tan, N. Mathews, T. Cahyadi, F. R. Zhu, S. G. Mhaisalkar, *Appl. Phys. Lett.* **2009**, *94*, 263303; c) J. Veres, S. D. Ogier, S. W. Leeming, D. C. Cupertino, S. Mohialdin Khaffaf, *Adv. Funct. Mater.* **2003**, *13*, 199-204.

[31] F. G. del Pozo, S. Fabiano, R. Pfattner, S. Georgakopoulos, S. Galindo, X. Liu, S. Braun, M. Fahlman, J. Veciana, C. Rovira, X. Crispin, M. Berggren, M. Mas-Torrent, *Adv. Funct. Mater.* **2016**, *26*, 2379-2386.

[32] J. Meyer, R. Khalandovsky, P. Görrn, A. Kahn, *Adv. Mater.* **2011**, *23*, 70-73.

[33] K. S. Park, S. M. Salunkhe, I. Lim, C.-G. Cho, S.-H. Han, M. M. Sung, *Adv. Mater.* **2013**, *25*, 3351-3356.

[34] X. Sun, L. Zhang, C. a. Di, Y. Wen, Y. Guo, Y. Zhao, G. Yu, Y. Liu, *Adv. Mater.* **2011**, *23*, 3128-3133.

[35] L. Viani, C. Risko, M. F. Toney, D. W. Breiby, J.-L. Brédas, *ACS Nano* **2014**, *8*, 690-700.

[36] a) R. A. Marcus, *Rev. Mod. Phys.* **1993**, *65*, 599-610; b) V. Coropceanu, J. r. m. Cornil, D. A. da Silva Filho, Y. Olivier, R. Silbey, J.-L. Brédas, *Chem. Rev.* **2007**, *107*, 926-952.

[37] G. R. Hutchison, M. A. Ratner, T. J. Marks, *J. Am. Chem. Soc.* **2005**, *127*, 2339-2350.

[38] S. C. B. Mannsfeld, A. Virkar, C. Reese, M. F. Toney, Z. Bao, *Adv. Mater.* **2009**, *21*, 2294-2298.

[39] Bearing in mind the effect of the deposition rate, all the samples were sublimed under identical conditions (see Experimental section).

[40] a) J. Locklin, M. E. Roberts, S. C. B. Mannsfeld, Z. Bao, *J. Macromol. Sci., Polym. Rev.* **2006**, *46*, 79-101; b) S. Y. Yang, K. Shin, C. E. Park, *Adv. Funct. Mater.* **2005**, *15*, 1806-1814.